Original Article
Tolypothrix Dichloromethane Ethylacetate fraction (TDEF) inhibits cisplatin resistance H357 cell through PI3K/AKT/beta-catenin pathway

Rameshwari Heisnam[1,2], Soibam Thoithoisana Devi[1,3], Sibasish Mohanty[4], Pulok K Mukherjee[1], VVS Prasanna Kumari Rayala[5], Pullapanthula Radhakrishnanand[5], Rupesh Dash[4], Nanaocha Sharma[1]

[1]Microbial Resources Division, Institute of Bioresources and Sustainable Development (An Autonomous Institute under Department of Biotechnology, Govt. of India), Takyelpat, Imphal 795001, Manipur, India; [2]School of Biotechnology, Kalinga Institute of Industrial Technology, Deemed To Be University, Bhubaneswar 751024, Odisha, India; [3]Department of Zoology, Manipur University, Imphal 795003, Manipur, India; [4]Institute of Life Sciences (ILS), Bhubaneswar 751023, Odisha, India; [5]National Institute of Pharmaceutical Education and Research (NIPER), Guwahati 781039, Assam, India

Abstract: Chemoresistance is one of the major factors for treatment failure in OSCC. Reprogramming chemoresistance cells to undergo drug induced apoptotic cell death is a feasible approach to overcome drug resistance. Cyanobacteria is considered important sources of lead compounds for the development of drugs for treating cancer chemoresistance. This study deals with the role of Tolypothrix Dichloromethane Ethyl acetate fraction (TDEF) inducing apoptosis in cisplatin resistance H357 cell (H357cisR) and the underlying mechanisms sensitizing the chemoresistance. TDEF showing effective activity against H357cisR with IC_{50}-14.13±1.18 µg mL^{-1}, inhibits proliferation and migration. Proteome apoptosis arrays were found to stimulate phosphorylation of p53, activation of proapoptotic proteins including BAX and cytochrome C (CYCS), caspase-3/9 (CASP3/9), suppression of anti-apoptotic proteins like Bcl2, survivin and increased expression of the cell cycle checkpoint protein p21, p27. TDEF induced apoptosis with cell death-transducing signals, that regulate the Matrix metalloproteinases (MMPs) by down-regulation of Bcl2 and up-regulation of Bax, triggering the cytochrome c release from mitochondria to cytosol thus triggered the activation of caspases-9 to activate downstream executioner caspase-3/7 required for apoptotic changes. The mechanistic pathway of apoptotic cell death in H357cisR was done through inhibiting β-catenin through GSK3β in turn activated by AKT. The phosphorylated β-catenin leads to proteasome degradation and unable to translocation to nucleus thereby activating c-Myc, survivin, Cyclin D and upregulate p21 expression which lead to cell cycle arrest in G_0/G_1 phase.

Keywords: H357cisR, antibody array, β-catenin, p21, chemoresistance

Introduction

According to data from the Global Cancer Observatory (GCO), there were 3,77,713 OSCC cases annually in 2020, with Asia recording the most instances (2,48,360), followed by Europe (65,279) and North America (27,469). More than one-third of new cases (1,35,929) and one-fifth of deaths (75,290) are attributable to India alone [1].

Radiation treatment and surgery are the main therapeutic modalities used to treat OSCC. For OSCC tumours that cannot be physically removed, neoadjuvant CT is typically advised [2]. Chemotherapeutic drug resistance may develop as a result of innate or acquired mechanisms. In contrast to acquired mechanisms, which take place later in cancer treatment and result in tumour cells that were initially sensitive to the chemotherapeutic agent being administered developing resistance against it, intrinsic mechanisms develop resistance naturally to chemotherapeutic drugs at the onset of treatment [3, 4]. The chemoresistance cell experience increase cancer stem cell popula-

tion, decreased drug accumulation, drug-target interaction, apoptotic response, and increased autophagy activity which leads to high chance of tumour recurrence [5].

Therefore, reprogramming resistant cells experiencing drug induced cell death has become the possible strategy to overcome drug resistance. Natural products such as medicinal plants and blue green algae extract play a significant role in rewiring chemoresistance cell by inducing apoptosis. Filamentous cyanobacteria contain a great variety of compounds that are potentially exploitable for extracting bioactive substances that effectively kill cancer cells by inducing apoptotic death [6]. Cyanobacteria produce several compounds to induce apoptotic death, and compounds like synthadotin [7], cryptophycin [8], and curacin [9] were already identified with their anticancer effect; some of these compounds have succeeded in entering the clinical trial also [10]. They have been reported to prevent cancer growth and neurodegenerative and infectious diseases [11]. *Tolypothrix* is a heterocystous filamentous cyanobacteria that belong to the order Nostocales and occurs in fasciculated colonies mostly found in floating tufts or submerged in fresh torpid water attached to plants or rock surfaces. Tolytoxin isolated from *Tolypothrix* specifically can alters the microfilament organization of cells by preventing actin polymerization [12].

Early apoptotic cell express phosphatidylserines (PS) on the plasma membrane's outer leaflet and stained using the annexin V marker. Late apoptotic and necrotic cells lose the integrity of their cell membranes, making them permeable to essential dyes like 7-AAD, Propidium iodide (PI) [13]. Apoptosis assay measures the biological events connected to programmed cell death, such as DNA fragmentation, phosphatidylserine (PS) exposure on the cell surface, and caspase activation. Using the annexin V/7-amino-actinomycin stain, it is simple to distinguish between early and late apoptosis as well as necrosis.

The activation of p53, a transcription factor, promotes apoptosis through the transcription of its target genes, such as Bcl-2 family members [14, 15]. Anti-apoptotic proteins such as BCL-2, BCL-XL, MCL-1, BCL-W, and A1/BFL1 are inhibited by the BH3-only proteins upon activa-

tion of BAX/BAK. This leads to the permeabilized of the mitochondrial outer membrane triggering the recruitment of caspase and its activator APAF-1 [16], which destroys the cell. But the extrinsic pathway recruits and activates caspase-8 via the adaptors FADD and TRADD [17, 18] and accumulates death receptors in the plasma membrane to cause apoptosis.

One of the crucial connections between external stimuli and essential cellular functions is the activated phosphatidylinositol 3-kinase (PI3K)/Akt pathway, which is critical for the proliferation, apoptosis, and survival of tumor cells [19]. In many cancer types, including oral cancer, PI3K and Akt activation is a factors in medication resistance [20]. Additionally, Wnt/β-catenin signaling system is essential for cell homeostasis and embryonic development. It is also implicated in tumor cell proliferation, invasion, apoptosis, stemness, and treatment resistance. In the absence of a Wnt signal, serine/threonine kinases, casein kinase I (CKI), and GSK3β phosphorylate free cytoplasmic β-catenin, targeting it for destruction via the proteasome and lowering the levels of β-catenin in the cytoplasm [21, 22]. Wnt signaling disrupts this degradation complex, and GSK3β dissociation prevents β-catenin from being phosphorylated and keeps it stabilized in the cytoplasm. The stabilized β-catenin in the cytoplasm is able to go into the nucleus and form a complex with T-cell factor/lymphoid enhancer factor (TCF/LEF) proteins; it induces the transcription of genes involved in cell growth and proliferation, such as c-myc, cyclin D1, and survivin [23, 24]. The present study aimed to identify the mechanism behind the chemoresistance cell H357cisR cell death induced by TDEF.

Materials and method

Cyanobacteria extract preparation

By following Doan et al., method, extraction was done in 40-45 d old batch cultures [25]. For extract preparation, 500 mg of dried biomass was mixed with 500 μL of CH_2Cl_2, and Met OH. The extract was macerated in a homogenizer and reflux extraction using CH_2Cl_2/Met OH (2:1) solvent ratio. After 48 hrs, the solvent was filtrated, and the extract was concentrated in a rotary vacuum evaporator at 40°C. The dried residues were dissolved in dimethyl sulfoxide (DMSO) for evaluation of cell cytotoxicity.

Column chromatography

A portion of the extract was subjected to bioactivity-directed silica column chromatography of silica gel (60-120 mesh). Different solvent systems of increasing polarity comprising hexane, Dichloromethane, ethyl acetate, and methanol served as mobile phases and eluted gradient with Hex (100%, v/v), Hex:CHCl3 (80:20% to 20:800%, v/v), $CHCl_3$ (100%, v/v), $CHCl_3$:EtAc (80:20% to 20:80%, v/v), EtAc (100%, v/v), EtAc:EtAc (80:20% to 20:80% v/v), EtAc (100%, v/v), EtAc:MeOH (80:20% to 20:80%, v/v) and finally MeOH (100%, v/v), yielding 16 fractions [26]. The cytotoxic activity of 16 fractions was analyzed using an MTT assay on the H357 cancer cell line. The highest cell death potential fraction was further checked its cell viability against H357cisR cells.

Instrumentation and analytical conditions (LC-MS)

The phytochemicals were examined using a 1290 Infinity HPLC System that was coupled to a 6545 Q-TOF (Agilent Technologies, Santa Clara (CA), USA). For the chromatographic separation of all metabolites, a Phenomenex Kinetex 5 μm EVO C18 100A° column with an inner diameter of 1.6 mm and a length of 250 mm was utilised. The parameters for the column used were 35°C temperature, 5 μL injection volume, and a steady flow rate of 0.600 mL/min. Metabolite separation was carried out by gradient technique with the mobile phase consisting of (A) 0.1% formic acid in water and (B) methanol. The gradient was carried out by starting with 5% B for 0-5 minutes, linearly increasing B in a gradient from 5% to 100% B for 5.1-25 minutes, maintaining 100% B for 40 minutes, and then moving back to 5% B to equilibrate the column for 30-40 minutes.

The following settings were optimised for MS and MS/MS scans under typical operating source conditions. The temperature of the gas source is 320°C, the sheath gas temperature is 350°C, the drying gas rate is 10 L/min, the nebulizer pressure is 40 psig, the spray voltage is 3500 V, and so on. For MS investigations, both positive and negative ionisation techniques with m/z ranges of 50 to 1700 were employed. For the purpose of collecting MS data, scan rates of 1.0 scans per second were employed in both positive and negative modes.

Anticancer activity by MTT assay

H357 was obtained from sigma Aldrich, procured from European collection of authenticated cell culture and H357cisR cell was maintained in ILS Bhubaneswar. Cells were incubated on Dulbecco's Modified Eagle Medium F12 (DMEM F12) enriched with 10% fetal bovine serum and 2% penicillin Streptomycin and 10 ug mL^{-1} hydrocortisone. Cell lines were maintained as monolayers in T75 cell culture flasks with filter screw at 37°C in a humidified 5% CO_2 incubator. Cells were treated with TDEF and performed MTT assay as follows [27]. The absorbance given from each well was read at a wavelength of 570 nm in a multi-plate reader. Graph Pad prim 8.2 was used to calculate the percentage of relative viability and the half-maximal inhibitory concentration IC_{50}.

AnnexinV/7AAD apoptosis assay

Cells were harvested and stained using with Annexin V and PI according to the manufacturer's recommendations. Briefly, the cells were trypsinized, washed in PBS, and resuspended in binding buffer (1×10^6/mL). Equal volumes of Annexin V PE & 7AAD (Catalog 88-8102-74, eBioscience™) were added and incubated for 15 min at room temperature in the dark and analyzed by flow-cytometry. Cells were gated and analyzed for doublet discrimination. A population of single cells was acquired at excitation (490 nm) and emission (630 nm) wavelengths [28]. Data analysis was performed using BD FACS Software (BD Biosciences) to identify the percentage of cells in different phases of the cell cycle.

Cologenicity assay

H357cisR 400 cells/well were seeded in a 6-well culture plate and treated with 1, 2, and 3 μg mL^{-1} for 18 days in DMEM/F12 medium. After 18 days, visible colonies were stained with 0.5% crystal violet, and images were captured in Chemi XRS Gel Documentation System (Bio-Rad) [29].

Wound-healing

H357cisR cells were seeded at a density of 5×10^5 cells per well in a 24-well flat-bottom culture plate (BD Falcon). Cells were incubated with the indicated concentration of drugs in

DMEM/F12 medium supplemented with 10% FBS at 37°C [29]. When cells reached 90% confluence, wounds were created using p-10 pipette tips and washed 3 × with 1 × PBS. Images at zero time points (t = 0 hour) were captured to record the initial area of the wounds and recovery images of the wounded monolayers were captured at 12-hour time intervals for 48 hours when complete healing of the wound area was found in one of the groups. Images were captured in the LEICA DMIL microscope and processed by LEICA LAS V4.2 software.

Cell cycle analysis

H357 cells (2 × 10⁵) were seeded in a 6-well plate incubated in a CO_2 incubator for 24 hrs at 37°C. Cells were treated in different fraction concentrations of TDEF and further incubated for 48 hrs. Cells were rinsed twice with cold PBS, trypsinized, and harvested by centrifuging at 2000 rpm for 5 mins. The PBS rinsed cell pellet was fixed in ice-cold 70% ethanol overnight or 2 hrs at -20°C. Fixed cells were rinsed in cold PBS and stained for 15 minutes at 37°C in the dark using 0.1% (v/v) Triton X-100 in PBS, 200 g/ml DNAse-free RNAse A, and 20 mg/ml propidium Iodide [30]. Afterward, the *Tolypothrix*-treated H357 cells were stained with PI, and the cell distribution in different cell cycle phases was analyzed by FACS Flow cytometer.

Protein array analysis

Human apoptosis array analysis was performed using a proteome profiler apoptotic array kit (ARY009; R & D system. Minneapolis, MN, USA). The experiment proceeded according to the manufacturer's instructions. In short, H357cisR cells were treated with control and 10 ug mL⁻¹ of TDEF. After 24 hrs, cells were lysed gently with lysis buffer 6 and vortex for 30 min at 4°C. The human apoptosis array nitrocellulose membrane was blocked with blocking. Following the release of the unbound proteins, three items of washing with washing buffer were performed on the arrays and then incubated with a mixture of biotinylated detection antibodies and streptavidin-HRP antibodies with constitutive washing. The Image J software detected protein spot densities using the chemiluminescence detection reagents included in the Array Kits. Then the relative change of apoptotic protein in the treated sample with respect to the control was determined.

Western blotting

H357cisR cancer cells were treated with TDEF (5, 10, and 15 µg/mL) for 48 hrs. Cells were lysed using RIPA buffer, and whole cell lysates were collected after centrifugation at 12,000 rpm for 30 min at 4°C. Equal amounts of cell lysates were loaded for immunoprecipitation or immunoblotting using the indicated primary antibodies. The protein sample was separated by 5-12% SDS-PAGE, transferred to a nitrocellulose membrane and blocked with 5% skimmed milk and BSA for 1 h, and incubated with primary antibodies (1:1000 dilution) at 4°C overnight and then with secondary antibody (1:5000 dilution) for 1 h at room temperature. The blots were detected using a chemiluminescent ECL system. Using ImageJ software, the band intensity of each immunoblot (n = 3) was measured. Under the immunoblots, a mean band intensity value is shown. Each blot's intensity was calculated by normalizing it to the intensity of the β-actin blot [31].

Statistics

All data are presented as mean and standard deviation calculated using GraphPad Prism 8.2. The statistical significance was calculated by one- and Two-way ANOVA, and a *P* value of less than or equal to 0.05 was considered significant.

Results

Tolypothrix column fraction Dichloromethane:Ethylacetate showing the effective cytotoxic activity against H357cisR

Tolypothrix filamentous cyanobacteria was extracted using Dichloromethane:Ethylacetate (2:1), the crude extract was further fractionated through Bioassay guided column fractionation. Hexane, Dichloromethane, Ethylacetate and Methanol were used in different solvent ratio and 16 different column fractions were collect. The active metabolites present in *Tolypothrix* crude extract and column fraction target cancer cell growth of H357 was determined by cell viability or MTT assay. Each one of the fractions treated against H357 and determined the cell viability percentage of all the column fraction.

Table 1. Cell treated with TDEF after 48 hrs were determined for cell viability using MTT reagent and absorbance was taken at 570 nm

Sl.no.	Column fraction	IC_{50} (ug mL^{-1})
1	A: 100% hexane	547.58±7.86
2	B: Hexane:Dichloromethane (80:20)	540.74±7.8
3	C: Hexane:Dichloromethane (60:40)	246.92±6.06
4	D: Hexane:Dichloromethane (40:60)	179.27±1.23
5	E: Hexane:Dichloromethane (20:80)	150.58±6.83
6	F: 100% dichloromethane	117.30±6.07
7	G: Dichloromethane:Ethylacetate (80:20)	139.09±5.44
8	H: Dichloromethane:Ethylacetate (60:40)	148.64±3.24
9	I: Dichloromethane:Ethylacetate (40:60)	31.99±3.03
10	J: Dichloromethane:Ethylacetate (20:80)	43.10±3.76
11	K: 100% Ethylacetate	59.73±3.77
12	L: Ethylacetate:Methanol (80:20)	85.25±3.67
13	M: Ethylacetate:Methanol (60:50)	258.26±6.18
14	N: Ethylacetate:Methanol (40:60)	344.94±7.41
15	O: Ethylacetate:Methanol (20:80)	812.89±6.37
16	P: 100% Methanol	330.06±7.73

Cell viability assay of 16 Tolypothrix column fraction were showing with their respective IC_{50} against H357 oral cancer cell line.

Then calculate the IC_{50} of 16 fraction using Graphpad Prism (**Table 1; Figure 1A**). Among them Dichloromethane and ethyl acetate (40:60) fraction show a significant cell cytotoxicity against H357.

Dichloromethane:Ethylacetate (40:60), an effective fraction against H357, was used to treat H357cisR cells, whose drug response was low due to intensive cisplatin treatment. TDEF has IC_{50} of 31.14±3.29 ug mL^{-1} in H357, whereas the reaction of those fraction to cell viability against H357cisR showed a more effective cell death with IC_{50}-14.13±1.18 ug mL^{-1} (**Figure 1B**). While the anti-proliferative activity of TDEF against H357cisR was found significant in 48 hrs where the activity was quite similar in case of 72 hrs treatment (**Figure 1C**).

The comparative study of TDEF in H357cisR and H357cisS shows the increase activity of TDEF in H357cisR cell and results showed that the activity of TDEF is far more significant than crude extract (**Figure 1D**). And TDEF has negligible cytotoxicity effect with IC_{50}-455± 1.20 ug mL^{-1} against Human Embryonic Kidney (HeK293) after incubation of 48 hrs (**Figure 1E**). This showed that TDEF would have poten-

tial to sensitised chemoresistance activity in H357cisR cell. Henceforth, we evaluated TDEF could restore cisplatin mediated cell death. The cell viability and cell death assay suggest that TDEF induced cisplatin mediated cell death in H357cisR. And further performed combinational treatment of TDEF and cisplatin showing significantly lower cell viability in case of combinational treatment as compare to treatment of cisplatin and TDEF alone (**Figure 2A**, **2B**). These data suggested the restoration of cisplatin activity against H357cisR cell while combining TDEF and cisplatin.

Additionally, we performed colony forming assay with low concentration of extract and analysing its proliferative activity. The one with the highest concentration of 3 µg mL^{-1} was showing significant reduced in colony no. as compare to control (**Figure 3A**). TDEF treated H357cisR cell showing anti migration potential as wound closure are significant and the percentage of wound closure showed in dose and time dependent manner (**Figure 3B**, **3C**). This result indicates the potential ability of TDEF to act as effective anti-proliferative and anti-migrating agents.

TDEF induces apoptotic cell death by arresting the proliferation of H357cisR cell

When TDEF treated to H357cisR, the cells change its morphology to round in shape and start detaching away from the surface at higher concentration (**Figure 4A**). Annexin V/7AAD apoptosis assay kit was used to determine the percentage of early and late apoptosis. TDEF treated H357cisR cells showing drug-induced apoptosis in a dose-dependent manner (**Figure 4B**). A graph of TDEF induced apoptosis in H357cisR was plotted against cell death (early apoptosis and late apoptosis) versus concentration (**Figure 4C**).

In order to undergo uncontrol proliferation of cell division in cancer cell line, cell needs to divide rapidly but our extract TDEF inhibit the cell proliferation inducing cell cycle arrest. There are three phases in cell cycle G1, S and G2 phase. TDEF treated H357cisR cell arrest
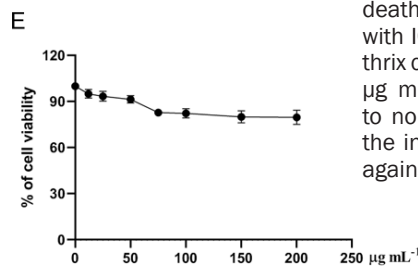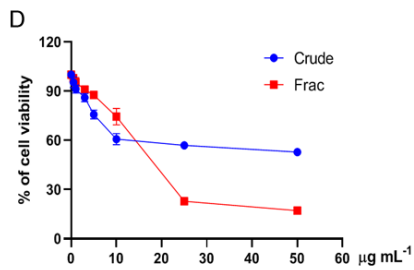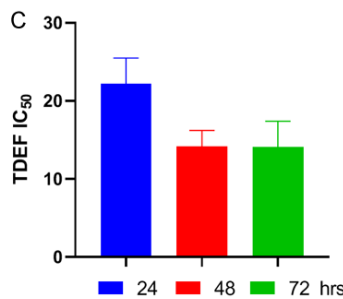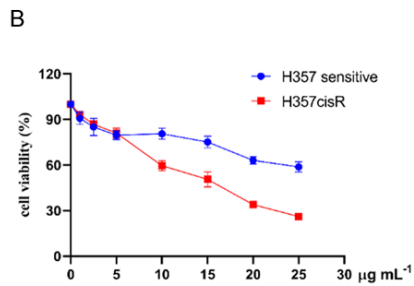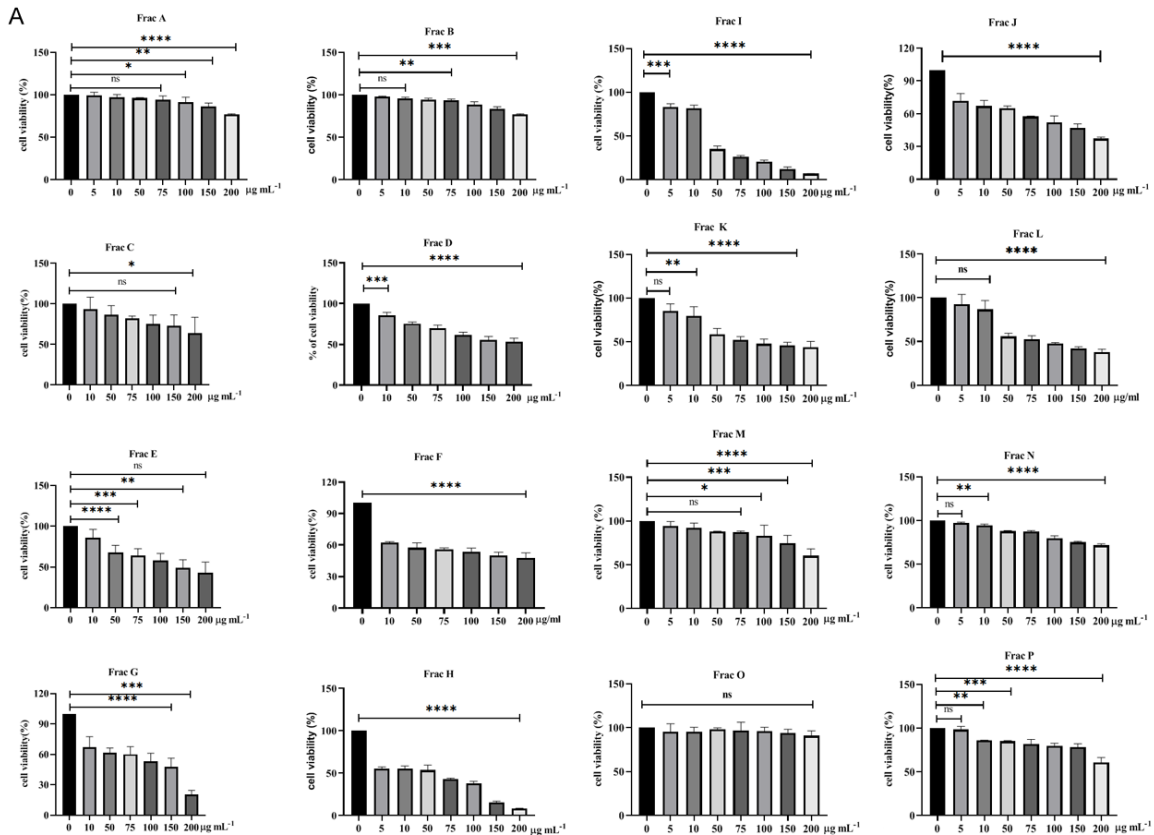
Figure 1. A. Cell viability assay graph of 16 column fractions showing with their respective IC$_{50}$ against H357 oral cancer cell line. B. Graph of cell viability assay of TDEF against oral cancer cell line H357 sensitive and H357cisR. C. With respect to time, the cell viability decreased, but cell viability was almost similar in 48 hrs and 72 hrs. D. Tolypothrix column fraction TDEF showing significant cell death activity against H357cisR cell with IC$_{50}$-14.13 µg mL^{-1} While Tolypothrix crude having IC$_{50}$ of 43.34±3.04 µg mL^{-1}. E. TDEF showing non-toxic to normal cell line Hek293 treating the indicated concentration of TDEF against HeK293 for 48 hrs.

the cell cycle on G1 phase which was 17.3% more compare to control (**Figure 4D**).

LC-MS/MS analysis of TDEF

TDEF was subjected to LC-MS/MS to identify the metabolites responsible for the anticancer activity. Compounds detected in the positive mode with anticancer properties were Canthaxanthin [32], Dragonamide [33], Neurosporaxanthin [34], C16-sphingosine [35] were detected in the positive mode while D-Mannitol [36], Tetraconazole [37] and Tocotrienols [38] are detected in negative mode. 3-O-Methylgallate [39], Phloroglucinol [40] and 6-Paradol [41] were detected in both positive and nega-
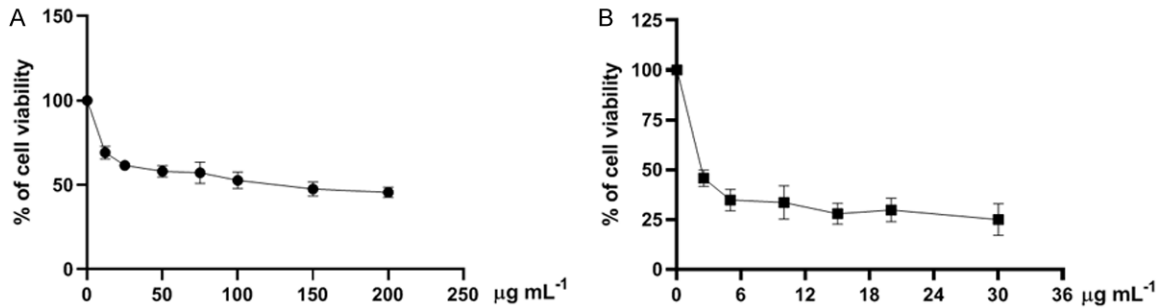
Figure 2. TDEF restored cisplatin-induced cell death in chemoresistant OSCC. (A) Cell viability of cisplatin against H357cisR cell and (B) Chemoresistant cell H357 CisR cells were treated with cisplatin 120 µg mL^{-1} and indicated concentration of TDEF for 48 hrs, after which cell viability was determined by MTT assay (Mean ± SEM, n = 3).

tive modes. The TDEF total metabolites detected using LC MS was shown in Suplementary Table 1. The total anticancer compounds detected in the positive and negative modes are listed in **Table 2**.

Antibody based apoptosis array screen reveal p53 mediated apoptosis and upregulation of p21

The potential molecular mechanisms responsible for the apoptotic activity were analyzed using a proteome profile array to evaluate 35 apoptosis-associated proteins. In this study, we aimed to examine the dominant signalling cascades and apoptotic mediators during TDEF mediated cytotoxicity. Firstly, the cells were treated with 10 ug mL^{-1} extract concentration for 48 hrs, and total cell extracts were isolated and subjected to human apoptosis array analysis. Overall, the results indicated that the p21, cytochrome C and Pp53 showed the greatest fold increase in apoptosis (with P21 increased 4.91-fold, Cytochrome C 2.29-fold, and Pp53 2-fold), as compared with the untreated control (**Figure 5A**, Suplememtary Table 2). Other proteins also showed increased protein expression of cleaved caspase3 (1.49 fold). On the other hand, the protein expression of anti-apoptotic proteins like Bcl2 survivin was significantly decreased (**Figure 5B**).

TDEF regulate the expression of p53 in cisplatin resistance oral cancer cell line H357cisR

As per the above result, TDEF treated H357cisR cells induced apoptosis. The result is further validated by immunoblotting of apoptosis-related protein and analyzing its expression.We found that pAKT and MDM2 minimal expres-

sion while p53 got activated as MDM2 minimal expression unable to phosphorylate p53 for proteosomal degradation (**Figure 6**). Immunoblotting data showed that when administrating TDEFH357cisR cells substantially increased cisplatin-induced cleaved poly (ADP-ribose) polymerase (PARP), Cleaved caspase 3, γ-H2AX expression and inactivation of anti-apoptotic proteins like Bcl2, survivin, and MCL1 which are proteins of p53 downstream pathway.

TDEF induces inactivation of the canonical Wnt pathway

TDEF treated cell protein lysate was isolated and used for immunoblotting study employing antibody of identified key players in the canonical Wnt pathway, including pGSK3B, cytosolic β-catenin, nuclear β-catenin, cyclin D1, and c-myc. When compared to controls, pGSK3b, phosphoβ-catenin, and cyclin D1 protein levels were lower after a 48-hour TDEF treatment. As AKT unable to inactivate GSK3β, β-catenin degradation takes place which in turn prevents cMyc and cyclin D from being transcribed and boosts the production of p21 (**Figure 7**).

Discussion

Due to the widespread use of chemotherapeutic medications, chemotherapy resistance is a significant limiting factor in the treatment of cancer. As a result, despite the market's abundance of cancer medications, treatment success rates are still poor. Chemotherapy-resistant cancer cells have large quantities of anti-apoptotic proteins. Therefore, it's critical to reestablish apoptosis in chemotherapy-resistant tumour cells.
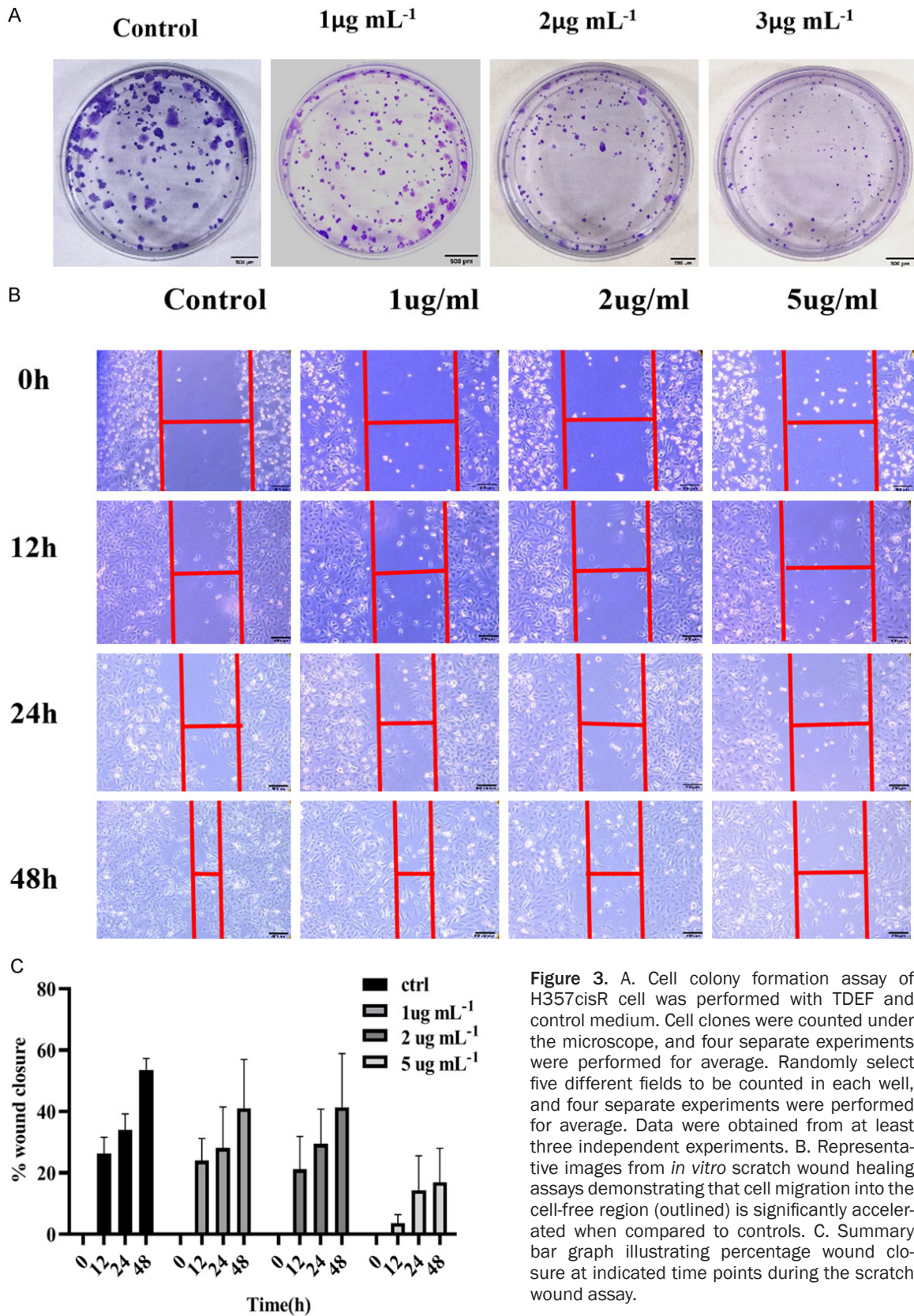
Figure 3. A. Cell colony formation assay of H357cisR cell was performed with TDEF and control medium. Cell clones were counted under the microscope, and four separate experiments were performed for average. Randomly select five different fields to be counted in each well, and four separate experiments were performed for average. Data were obtained from at least three independent experiments. B. Representative images from *in vitro* scratch wound healing assays demonstrating that cell migration into the cell-free region (outlined) is significantly accelerated when compared to controls. C. Summary bar graph illustrating percentage wound closure at indicated time points during the scratch wound assay.
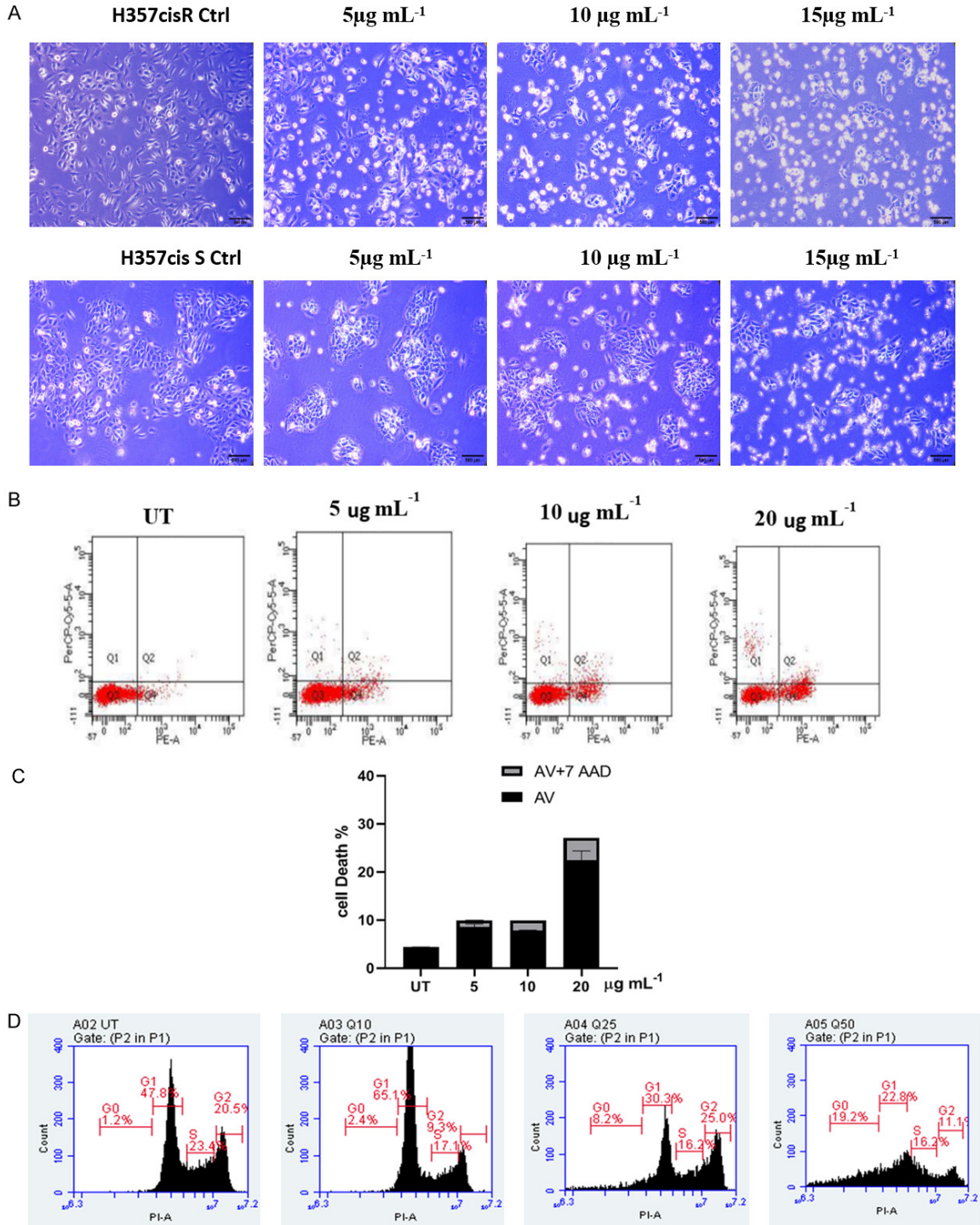
Figure 4. A. Oral cancer cell line H357 sensitive and H357cisR was seeded on 6 well plates and treated with different concentrations 5, 10, and 15 ug mL^{-1}. With respect to time, the cell morphology changes and becomes rounded in shape, and at higher concentration cell starts to detach from the surface. B. H357CisR cells were treated with indicated dose of TDEF for 48 hrs after which cell death was determined by annexin V/7AAD assay using flow cytometer. The dot plots represent the percentage of early apoptotic (lower right) and late apoptotic cells (upper right). C. Bar diagrams indicate the percentage of cell death; black color portion indicates percentage of early apoptosis and grey color indicates percentage of late apoptosis occur with respective treated groups. D. TDEF treated H357cisR cell pellet was fixed with 70% ethanol and stained with propidium iodide and the cell distribution in different cell cycle phases was analyzed by FACS. Cell cycle arrest was shown highest at 10 ug mL^{-1} but the cell with the higher concentration of extract has experience apoptosis and necrosis. The percentage of the G1 population was found to be 65.1%, and the control G1 cell population was 47.8%.

Table 2. List of the TDEF metabolites identified using LC MS

a) Positive mode

Sl.no.	Name	Mass	RT	Height	Area	Score	Formula	m/z	Diff (Tgt, ppm)
1	Canthaxanthin	564.396	26.64	1811983	39898460	98.95	$C_{40}H_{52}O_2$	565.404	-0.59
2	6-Methoxymellein	208.073	20.08	10978	76580	82.96	$C_{11}H_{12}O_4$	209.08	-3.73
3	4H-Cyclopenta[def]chrysene	240.095	15.42	1166	14650	75.27	$C_{19}H_{12}$	241.103	3.92
4	Azithromycin	748.509	31.68	359947	4024774	99.52	$C_{38}H_{72}N_2O_{12}$	749.516	0.68
5	Hydroxytyrosol 1-O-glucoside	316.116	17.88	1265	16452	77.67	$C_{14}H_{20}O_8$	317.123	-0.45
6	Carvone oxide	166.099	22.08	2431	110462	77.57	$C_{10}H_{14}O_2$	167.106	-5.55
7	Gamma Glutamylglutamic acid	276.097	22.36	6346	49843	81.11	$C_{10}H_{16}N_2O_7$	277.104	4.17
8	Citalopram	324.165	17.23	3918	44325	77.37	$C_{20}H_{21}FN_2O$	325.173	4.81
9	Demethoxyfumitremorgin C	349.179	15.92	90297	652159	91.17	$C_{21}H_{23}N_3O_2$	350.186	-0.83
10	Dezocine	245.179	17.42	2096	4005	76.01	$C_{16}H_{23}NO$	246.185	2.22
11	HMT-toxin	768.47	21.71	6599	108941	78.98	$C_{41}H_{68}O_{13}$	769.478	5.46
12	Hydroxytyrosol 1-O-glucoside	316.116	17.88	1265	16452	77.67	$C_{14}H_{20}O_8$	317.123	-0.45
13	Ivermectin B1b	860.491	22.13	1508	6212	77.12	$C_{47}H_{72}O_{14}$	861.495	-1.79
14	Methotrexate	454.173	16.55	1816	13584	75.59	$C_{20}H_{22}N_8O_5$	455.18	2.53
15	Neurosporaxanthin	564.396	26.66	1851791	39269957	99.35	$C_{40}H_{52}O_2$	565.404	-0.77
16	Phloroglucinol	126.032	3.78	6382	55041	86.67	$C_6H_6O_3$	125.024	0.16
17	Phytosphingosine	317.293	24.38	4652	49396	82.58	$C_{18}H_{39}NO_3$	318.3	-1.71
18	Scutellarein	286.048	17.22	2327	43163	82.12	$C_{15}H_{10}O_6$	287.055	0.48
19	Tacrolimus	803.481	27.99	15571	325418	95.89	$C_{44}H_{69}NO_{12}$	804.488	-1.86
20	Macrocarpal I	490.291	22.59	80371	474575	78.98	$C_{28}H_{42}O_7$	491.299	-3.76
21	Thioridazine	370.156	28.97	1605	18069	77.16	$C_{21}H_{26}N_2S_2$	371.163	7.23
22	Xanthyletine	228.079	26.49	13619	215260	85.64	$C_{14}H_{12}O_3$	229.087	2.12
23	Fortimicin KK1	366.211	21.54	74543	351950	92.05	$C_{14}H_{30}N_4O_7$	367.219	-0.62
24	PC (14:0/14:0)	678.504	22.54	561415	11781329	86.58	$C_{36}H_{73}NO_8P$	679.512	-4.78
25	8-Epiiridodial	168.115	22.99	22884	1085954	85.89	$C_{10}H_{16}O_2$	169.122	-1.82
26	C16 Sphinganine	273.267	22.18	106870	2101841	99.65	$C_{16}H_{35}NO_2$	274.274	-0.91
27	Kanzonol K	436.186	25.57	496725	4172304	84.23	$C_{26}H_{28}O_6$	437.193	-6.1
28	Dragonamide D	605.417	28.62	4561	83285	77.23	$C_{32}H_{55}N_5O_6$	606.425	3.19
29	Naphthalene dihydrodiol	162.068	27.19	326541	2670798	87.63	$C_{10}H_{10}O_2$	163.076	0.6
30	3-O-Methylgallate	184.0368	3.64	18361	271893	98.33	$C_8H_8O_5$	183.0296	-2.1
31	6-Paradol	278.1882	26.75	3307	27507	79.19	$C_{17}H_{26}O_3$	277.181	0.02

b) Negative mode

Sl.no.	Name	Mass	RT	Height	Area	Score	Formula	m/z	Diff (Tgt, ppm)
1	Stearic acid	284.271	30.56	61761	403125	92.22	$C_{18}H_{36}O_2$	283.2638	-1.85
2	D-Mannitol	182.0786	3.6	6787	61913	85.65	$C_6H_{14}O_6$	181.0713	-2.54
3	Gallic acid	170.0213	3.8	13253	118030	86.3	$C_7H_6O_5$	169.014	-1.59
4	Phloroglucinol	126.0317	3.78	6382	55041	86.67	$C_6H_6O_3$	125.0244	0.16
5	Tetraconazole	371.0217	26.84	1441	28283	84.41	$C_{13}H_{11}Cl_2F_4N_3O$	370.0142	0.37
6	Lithocholic acid	376.2994	27.83	26024	1743140	83.43	$C_{24}H_{40}O_3$	375.2924	4.47
7	Tocoretinate	712.583	29.61	10794	80051	81.46	$C_{49}H_{76}O_3$	711.5763	4.96
8	3-O-Methylgallate	184.0372	15.21	4218	277730	77.6	$C_8H_8O_5$	183.0299	0.09
9	6-Paradol	278.1882	26.75	3307	27507	79.19	$C_{17}H_{26}O_3$	277.181	0.02

However, in our study, TDEF treated H357cisR cell showing upregulation of proapoptotic protein and downregulation of anti-apoptotic protein. Similar to L. Yang et al., report that Cur treated H69AR cells showed high protein expression of pro-apoptotic proteins such as Bad, Bax, Caspase-3, TRAIL R1, TRAIL R2, FADD, Fas, SMAC/DIABLO, HMOX2 whereas Bcl-2, cIAP-1, CLU, and HIF1A; anti-apoptotic proteins were significantly decreased [42]. They also report the increase of cytochrome c release and cleaved caspase3 which are the crucial sign of mitochondrial mediated apoptosis [43]. Additionally, cytochrome C interacts to
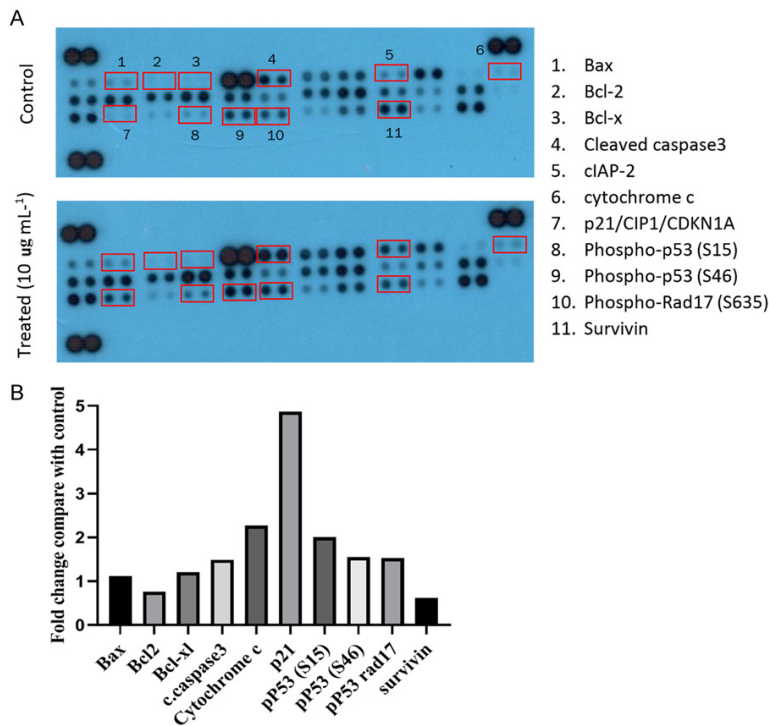
Figure 5. A. The Pp53 and P21 signalling pathways are strongly activated by TDEF treatment. The human apoptosis proteome profiler array used a protein extract (400 µg). The intensities of each array spot were visualized and further quantified using an image. B. The graph shows the relative fold change of proteins with significant differences upon TDEF treatment, setting 1 for control (no treatment of TDEF). Protein levels with higher than ± 2 folds are considered candidates for TDEF-induced cell death.

nogenesis through cell cycle control [45].

According to the findings of the apoptosis array profiling, p21 and p53 were the proteins with the highest fold changes. It has been reported that MDM2 can be phosphorylated at Ser166 and Ser186 by insulin-induced activated AKT (Ser473), which can lead to p53 being degraded by proteasomes both in the cytoplasm and the nucleus via MDM2 [46-48]. Therefore, the crucial p53 pathway proteins were examined using an immunoblotting evaluation, where pAKT and pMdm2 were found downregulated. Therefore, it can be deduced that inactive AKT is unable to phosphorylate MDM2 or p53 for proteosomal degradation, which causes p53 activation and transcript genes involved in apoptosis, including Bcl2, Bax, survivin, and bad cell cycle regulators like p21 and p27.

Apaf-1 during mitochondrial-mediated apoptosis to create the apoptosome complex. Further caspase 3 and other downstream caspases are activated when procaspase 9 binds to the apoptosome [44]. In harmony to the above report, TDEF induces loss of mitochondrial potential, supports that the overexpression of BAX and release of CYCS caused the mitochondrial malfunction to generate energy to the cell. This, in turn, stimulated the cleavage of CASP9/3 and PARP1. On the other hand, G1/S, G2/M cell cycle checkpoint proteins like Pp53, p21, and p27 are all overexpressed and cause cell cycle arrest. Immunoblotting results were analysed p21, pP53, Bax were found increases and antiapoptotic proteins like Bcl2, survivin, cyclin E found decreases. The intrinsic mitochondrial route is likely used to carry out the TDEF induced apoptosis, given the induction/cleavage of BAX/CYCS/CASP9/CASP3/PARP1. And the Tacrolimus metabolites detected from LC-MS/MS reported the inhibition of oral carci-

Similar to this, it has been shown that PI3K-Akt inhibition results in increased expression of p21 and p27 [49]. Therefore, the result emphasized that the upregulation of p53 as well as the cell proliferation repressor proteins, p27 and p21 proved to be the consequences of PI3K-Akt inhibition. According to our result, TDEF treatment caused p53-mediated cell death in H357cisR cells.

We further study more on chemoresistance reprogramming pathway so as cell death mechanism of TDEF-treated H357cisR cell. Literature search revealed that β-catenin is abnormally active in the majority of CRC patients [50, 51] and is crucial for maintaining CCS-like cells [52]. Hence, β-catenin become a crucial therapeutic target for cancer chemoresistance.

Additionally, EZH2 protein suppression results in an increase in p21cip1 expression, which ultimately induces cell cycle arrest in the G1/S
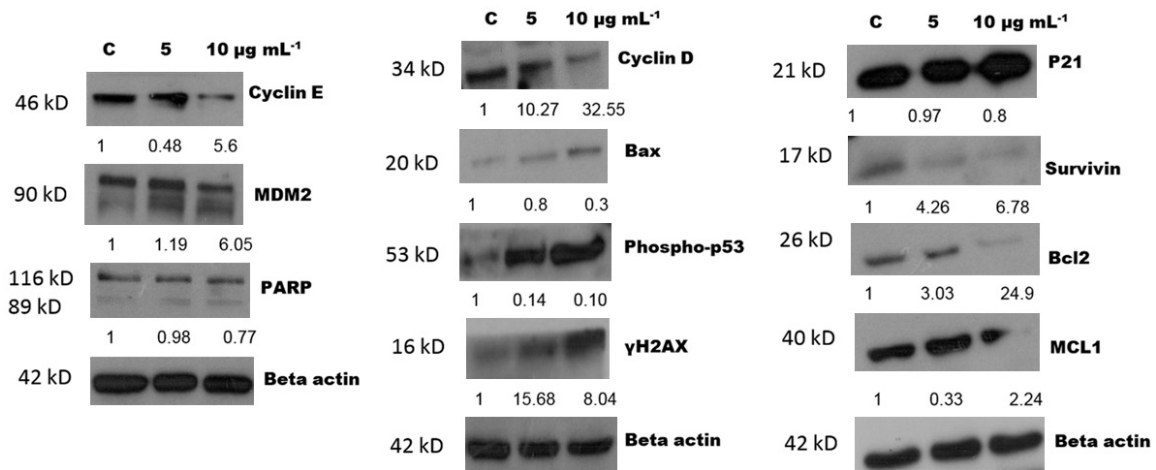
Figure 6. p53 expression is up-regulated in TDEF treated H357cisR cell against cisplatin chemoresistance oral cancer cell line H357cisR. Cell lysates were isolated and subjected to immunoblotting against indicated p53 regulated proteins and β-actin antibodies.
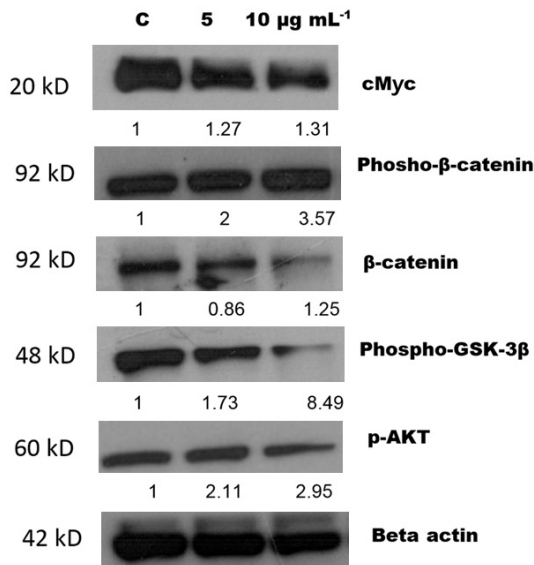
Figure 7. Activation of GSK3β followed by reduced expression of active β-catenin in cisplatin-resistant lines H357cisR were found in immunoblotting studies with indicated antibodies.

phase and inactivates the Wnt/β-catenin signalling pathway [53].

Our result is supported by the LC-MS/MS results which detected the presence of sphingosine [54] and γ-Glutamyl hydrolase [55] sensitized chemosensitivity of cancer cells.

Similarly, our proteome profiling and immunoblotting results showed the increase expression of P21 while β-catenin expression found decreases and cell cycle arrest also observed

at the G1 phase of cell cycle. We further look into the signalling pathway of PI3K/AKT/Beta catenin pathway. AKT has a crucial role in controlling both cell survival and apoptosis which is phosphorylated by Phosphoinositide-3 kinase (PI3K)-phosphoinositide-dependent protein kinase-1 (PDK1). Numerous cellular activities, including cell metabolism, cell death, and cell survival, rely on GSK3β because it is a crucial effector of PI3K/AKT cellular signalling [56]. The PI3K-Akt pathway in oral cancer is known to promote β-catenin's nuclear translocation in OSCC through the Akt-mediated phosphorylation of GSK3β, according to the findings [57-59]. According to earlier research, GSK3β inactivation by LiCl caused β-catenin to become activated and then go into the nucleus [60].

Glycogen synthase kinase 3 β (GSK3β), casein kinase 1 (CK1), the tumor-suppressor protein adenomatous polyposis coli (APC), and axin form a multiprotein complex known as a "destruction complex" that phosphorylates β-catenin on residues Ser33/Ser37/Thr41 in the absence of Wnt ligands [21, 61]. By being phosphorylated, β-catenin is subjected to proteasome-mediated destruction, which lowers its concentration in the cytoplasm. Inhibition of β-catenin unable to transcript c-Myc, survivin, and cyclin D1 and controls the progression of the cell cycle and ultimately results in P21 upregulation which results to cell cycle arrest [62, 63].

Overall, the mechanistic pathway of cell death was found to proceed through inactivating AKT,
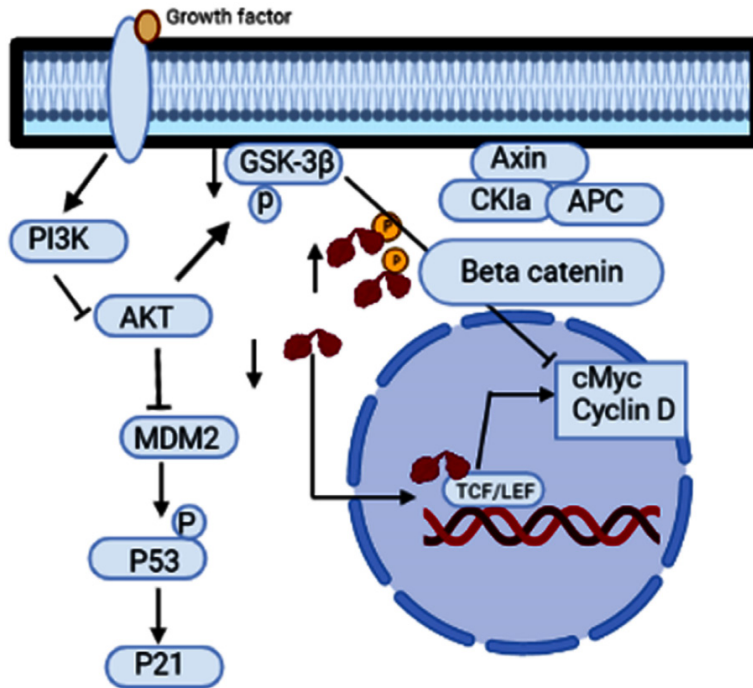
Figure 8. Schematic diagram showing TDEF induces cell death pathway in H357cisR chemoresistance oral cancer cell line.

ful role of p53 and AKT in TDEF induced apoptosis, cell cycle arrest and inhibition of β-catenin pathway in H357-cisR. The overall analysis of the result concluded that TDEFinduced cell death in H357cisR cells via the PI3K/AKT/Beta-catenin pathway. TDEF had the potential to sensitize chemoresistance oral cancer H357cisR. The promising results, together with the simple and cost-effective culturing and extraction technique, make these isolates quite plausible candidates as potential sources for chemotherapeutic anticancer drugs for the future. This fraction may be relevant for cancer therapeutic target for H357-cisR. Further study would provide more specific and less toxic drugs which would need preclinical animal model.

inducing activation of p53 results in to increase of P21 and, ultimately, cell cycle arrest. It also suppressed β-catenin pathway by inhibiting the phosphorylation of GSK3β. Inhibitionof β-catenin which in turn prevented the expression of cyclin D, survivin, and c-Myc (**Figure 8**).

TDEF treated H357cisR cell death undergoes in two different pathways of AKT: PI3K/AKT and AKT/beta catenin pathway. Inactivation of PI3K/AKT pathway results to activation of p53 pathway inducing apoptosis. While, inactivate of AKT blocked β-catenin translocation in nucleus thereby inactivate cell proliferation and ultimately blocked cell cycle arrest.

Conclusion

The present study proved that the Tolypothrix Dichloromethane Ethylacetate fraction (TDEF) showed effective cell death against H357cisR with an IC_{50} of 14.13±1.18 µg mL^{-1} which is more effective than H357. The extract shows anti-proliferative, anti-metastatic activity and also induces cell cycle arrest in the G1/S phase. The Proteome profiler array result depicts the high fold change in P21, cytochrome C and Pp53. Immunoblotting results shows an impact-

Disclosure of conflict of interest

None.

Abbreviations

DMEM F12, Dulbecco's modified Eagles medium F12; FBS, Foetal Bovine Serum; MMPs, matrix metalloproteinases; OSCC, Oral Squamous Cell Carcinoma; TDEF, Tolypothrix Dichloromethane Ethyacetate Fraction; PAK1,

p21 Activated Kinase 1; PBS, phosphate buffered saline; RIPA, Radioimmunoprecipitation assay; µgmL^{-1}, microgram per millilitre; IC$_{50}$, Half maximal inhibitory concentration; HRP, Horseradish peroxidase; CYCS, cytochrome C; SDS-PAGE, sodium dodecyl sulfate-Polyacrylamide gel Electrophoresis; BSA, Bovine serum albumin; ECL, Enhanced chemiluminescence; Pp53, phospho p53; MDM2, Mouse double minute 2 homolog; EZH2, Enhancer of zeste homolog 2; PDK1, Phosphoinositol dependent kinase 1; GSK3β, Glycogen synthase kinase-3 beta; CKI, casein kinase 1; APC, adenomatous polyposis coli.

Address correspondence to: Nanaocha Sharma, Microbial Resources Division, Institute of Bioresources and Sustainable Development (An Autonomous Institute under Department of Biotechnology, Govt. of India), Takyelpat, Imphal 795001, Manipur, India. E-mail: sharma.nanaocha@gmail.com; Rupesh Dash, Institute of Life Sciences (ILS), Bhubaneswar 751023, Odisha, India. E-mail: rupeshdash@ils.res.in

References

[1] Deo SVS, Sharma J and Kumar S. GLOBOCAN 2020 report on global cancer burden: challenges and opportunities for surgical oncologists. Ann Surg Oncol 2022; 29: 6497-6500.

[2] Pandey M, Kannepali KK, Dixit R and Kumar M. Effect of neoadjuvant chemotherapy and its correlation with HPV status, EGFR, Her-2-neu, and GADD45 expression in oral squamous cell carcinoma. World J Surg Oncol 2018; 16: 20.

[3] Mansoori B, Mohammadi A, Davudian S, Shirjang S and Baradaran B. The different mechanisms of cancer drug resistance: a brief review. Adv Pharm Bull 2017; 7: 339-348.

[4] Nikolaou M, Pavlopoulou A, Georgakilas AG and Kyrodimos E. The challenge of drug resistance in cancer treatment: a current overview. Clin Exp Metastasis 2018; 35: 309-318.

[5] Gupta PB, Onder TT, Jiang G, Tao K, Kuperwasser C, Weinberg RA and Lander ES. Identification of selective inhibitors of cancer stem cells by high-throughput screening. Cell 2009; 138: 645-659.

[6] Tan LT. Filamentous tropical marine cyanobacteria: a rich source of natural products for anticancer drug discovery. J Appl Phycol 2010; 22: 659-676.

[7] Ahmed W, El-Semary N, Abd El-Hameed O, El Tawill G and Ibrahim D. Bioactivity and cytotoxic effect of cyanobacterial toxin against hepatocellular carcinoma. J Cancer Sci Ther 2017; 9: 505-511.

[8] Tan LT. Bioactive natural products from marine cyanobacteria for drug discovery. Phytochemistry 2007; 68: 954-979.

[9] Martins RF, Ramos MF, Herfindal L, Sousa JA, Skærven K and Vasconcelos VM. Antimicrobial and cytotoxic assessment of marine cyanobacteria - Synechocystis and Synechococcus. Mar Drugs 2008; 6: 1-11.

[10] George BP and Abrahamse H. A review on novel breast cancer therapies: photodynamic therapy and plant derived agent induced cell death mechanisms. Anticancer Agents Med Chem 2016; 16: 793-801.

[11] Tan LT. Pharmaceutical agents from filamentous marine cyanobacteria. Drug Discov Today 2013; 18: 863-871.

[12] Berrendero E, Perona E and Mateo P. Phenotypic variability and phylogenetic relationships of the genera Tolypothrix and Calothrix (Nostocales, Cyanobacteria) from running water. Int J Syst Evol Microbiol 2011; 61: 3039-3051.

[13] Zimmermann M and Meyer N. Annexin V/7-AAD staining in keratinocytes. Methods Mol Biol 2011; 740: 57-63.

[14] Abdullah LN and Chow EK. Mechanisms of chemoresistance in cancer stem cells. Clin Transl Med 2013; 2: 3.

[15] Nakajima EC and Van Houten B. Metabolic symbiosis in cancer: refocusing the Warburg lens. Mol Carcinog 2013; 52: 329-337.

[16] Cecconi F, Alvarez-Bolado G, Meyer BI, Roth KA and Gruss P. Apaf1 (CED-4 homolog) regulates programmed cell death in mammalian development. Cell 1998; 94: 727-737.

[17] Varfolomeev EE, Schuchmann M, Luria V, Chiannilkulchai N, Beckmann JS, Mett IL, Rebrikov D, Brodianski VM, Kemper OC, Kollet O, Lapidot T, Soffer D, Sobe T, Avraham KB, Goncharov T, Holtmann H, Lonai P and Wallach D. Targeted disruption of the mouse Caspase 8 gene ablates cell death induction by the TNF receptors, Fas/Apo1, and DR3 and is lethal prenatally. Immunity 1998; 9: 267-276.

[18] Strasser A, Jost PJ and Nagata S. The many roles of FAS receptor signaling in the immune system. Immunity 2009; 30: 180-192.

[19] Heavey S, O'Byrne KJ and Gately K. Strategies for co-targeting the PI3K/AKT/mTOR pathway in NSCLC. Cancer Treat Rev 2014; 40: 445-456.

[20] Liu Y, Yang H, Chen T, Luo Y, Xu Z, Li Y and Yang J. Silencing of receptor tyrosine kinase ROR1 inhibits tumor-cell proliferation via PI3K/AKT/mTOR signaling pathway in lung adenocarcinoma. PLoS One 2015; 10: e0127092.

[21] MacDonald BT and He X. Frizzled and LRP5/6 receptors for Wnt/β-catenin signaling. Cold Spring Harb Perspect Biol 2012; 4: a007880.

[22] Mikels AJ and Nusse R. Wnts as ligands: processing, secretion and reception. Oncogene 2006; 25: 7461-7468.

[23] Willert K and Nusse R. Wnt proteins. Cold Spring Harb Perspect Biol 2012; 4: a007864.

[24] Fuentes RG, Arai MA and Ishibashi M. Natural compounds with Wnt signal modulating activity. Nat Prod Rep 2015; 32: 1622-1628.

[25] Thanh Doan N, Rickards RW, Rothschild JM and Smith GD. Allelopathic actions of the alkaloid 12-epi-hapalindole E isonitrile and calothrixin A from cyanobacteria of the genera Fischerella and Calothrix. J Appl Phycol 2000; 12: 409-416.

[26] Hossain MA, Islam A, Jolly Y and Kabir M. A new flavonol glycoside from the seeds of Zea Mays. Indian J Chem 2006; 45: 1319-1321.

[27] Mosmann T. Rapid colorimetric assay for cellular growth and survival: application to proliferation and cytotoxicity assays. J Immunol Methods 1983; 65: 55-63.

[28] Shriwas O, Priyadarshini M, Samal SK, Rath R, Panda S, Das Majumdar SK, Muduly DK, Botlagunta M and Dash R. DDX3 modulates cisplatin resistance in OSCC through ALKBH5-mediated m^{6}A-demethylation of FOXM1 and NANOG. Apoptosis 2020; 25: 233-246.

[29] Shriwas O, Arya R, Mohanty S, Mohapatra P, Kumar S, Rath R, Kaushik SR, Pahwa F, Murmu KC, Majumdar SKD, Muduly DK, Dixit A, Prasad P, Nanda RK and Dash R. RRBP1 rewires cisplatin resistance in oral squamous cell carcinoma by regulating Hippo pathway. Br J Cancer 2021; 124: 2004-2016.

[30] Engelke LH, Hamacher A, Proksch P and Kassack MU. Ellagic acid and resveratrol prevent the development of cisplatin resistance in the epithelial ovarian cancer cell line A2780. J Cancer 2016; 7: 353-63.

[31] Mohapatra P, Shriwas O, Mohanty S, Ghosh A, Smita S, Kaushik SR, Arya R, Rath R, Das Majumdar SK, Muduly DK, Raghav SK, Nanda RK and Dash R. CMTM6 drives cisplatin resistance by regulating Wnt signaling through the ENO-1/AKT/GSK3β axis. JCI Insight 2021; 6: e143643.

[32] Palozza P, Maggiano N, Calviello G, Lanza P, Piccioni E, Ranelletti FO and Bartoli GM. Canthaxanthin induces apoptosis in human cancer cell lines. Carcinogenesis 1998; 19: 373-376.

[33] Balunas MJ, Linington RG, Tidgewell K, Fenner AM, Ureña LD, Togna GD, Kyle DE and Gerwick WH. Dragonamide E, a modified linear lipopeptide from Lyngbya majuscula with antileishmanial activity. J Nat Prod 2010; 73: 60-66.

[34] Parra-Rivero O, Barros MP, Prado MDM, Gil JV, Hornero-Méndez D, Zacarías L, Rodrigo MJ, Limón MC and Avalos J. Neurosporaxanthin overproduction by fusarium fujikuroi and evaluation of its antioxidant properties. Antioxidants (Basel) 2020; 9: 528.

[35] Grammatikos G, Schoell N, Ferreirós N, Bon D, Herrmann E, Farnik H, Köberle V, Piiper A, Zeuzem S, Kronenberger B, Waidmann O and Pfeilschifter J. Serum sphingolipidomic analyses reveal an upregulation of C16-ceramide and sphingosine-1-phosphate in hepatocellular carcinoma. Oncotarget 2016; 7: 18095-18105.

[36] Hägerström E, Lindberg L, Bentzen J, Brødbæk K, Zerahn B and Kristensen B. The nephroprotective effect of mannitol in head and neck cancer patients receiving cisplatin therapy. Clin Med Insights Oncol 2019; 13: 1179554918821320.

[37] Jeong SA, Song J, Ham J, An G, Song G and Lim W. Tetraconazole interrupts mitochondrial function and intracellular calcium levels leading to apoptosis of bovine mammary epithelial cells. Pestic Biochem Physiol 2023; 191: 105366.

[38] Aggarwal V, Kashyap D, Sak K, Tuli HS, Jain A, Chaudhary A, Garg VK, Sethi G and Yerer MB. Molecular mechanisms of action of tocotrienols in cancer: recent trends and advancements. Int J Mol Sci 2019; 20: 656.

[39] Park JK, Yoo MJ, Jang H, Park SY, Choi J and Seol JW. Methyl gallate suppresses tumor development by increasing activation of Caspase3 and disrupting tumor angiogenesis in melanoma. Evid Based Complement Alternat Med 2022: 6295910.

[40] Kim RK, Suh Y, Yoo KC, Cui YH, Hwang E, Kim HJ, Kang JS, Kim MJ, Lee YY and Lee SJ. Phloroglucinol suppresses metastatic ability of breast cancer cells by inhibition of epithelial-mesenchymal cell transition. Cancer Sci 2015; 106: 94-101.

[41] Jiang X, Wang J, Chen P, He Z, Xu J, Chen Y, Liu X and Jiang J. [6]-Paradol suppresses proliferation and metastases of pancreatic cancer by decreasing EGFR and inactivating PI3K/AKT signaling. Cancer Cell Int 2021; 21: 420.

[42] Ilhan S. Profile of apoptotic proteins after curcumin treatment by antibody array in H69AR lung cancer cells. Eur J Biol 2020; 79: 157-162.

[43] Yang CL, Ma YG, Xue YX, Liu YY, Xie H and Qiu GR. Curcumin induces small cell lung cancer NCI-H446 cell apoptosis via the reactive oxygen species-mediated mitochondrial pathway and not the cell death receptor pathway. DNA Cell Biol 2012; 31: 139-150.

[44] Pan ST, Li ZL, He ZX, Qiu JX and Zhou SF. Molecular mechanisms for tumour resistance to chemotherapy. Clin Exp Pharmacol Physiol 2016; 43: 723-737.

[45] Li Y, Wang Y, Li J, Ling Z, Chen W, Zhang L, Hu Q, Wu T, Cheng B, Wang Y and Xia J. Tacrolimus inhibits oral carcinogenesis through cell cycle control. Biomed Pharmacother 2021; 139: 111545.

[46] Glasgow WC, Hui R, Everhart AL, Jayawickreme SP, Angerman-Stewart J, Han BB and Eling TE. The linoleic acid metabolite, (13S)-hydroperoxyoctadecadienoic acid, augments the epidermal growth factor receptor signaling pathway by attenuation of receptor dephosphorylation. Differential response in Syrian hamster embryo tumor suppressor phenotypes. J Biol Chem 1997; 272: 19269-19276.

[47] Gilbert B, Ahmad K, Roos J, Lehmann C, Chiba T, Ulrich-Rückert S, Smeenk L, van Heeringen S, Maier TJ, Groner B and Steinhilber D. 5-Lipoxygenase is a direct p53 target gene in humans. Biochim Biophys Acta 2015; 1849: 1003-1016.

[48] Yang MH, Zang YS, Huang H, Chen K, Li B, Sun Y and Zhao XW. Arsenic trioxide exerts anti-lung cancer activity by inhibiting angiogenesis. Curr Cancer Drug Targets 2014; 14: 557-566.

[49] McDonald GT, Sullivan R, Paré GC and Graham CH. Inhibition of phosphatidylinositol 3-kinase promotes tumor cell resistance to chemotherapeutic agents via a mechanism involving delay in cell cycle progression. Exp Cell Res 2010; 316: 3197-3206.

[50] de Sousa E Melo F and Vermeulen L. Wnt signaling in cancer stem cell biology. Cancers (Basel) 2016; 8: 60.

[51] Easwaran H, Tsai HC and Baylin SB. Cancer epigenetics: tumor heterogeneity, plasticity of stem-like states, and drug resistance. Mol Cell 2014; 54: 716-727.

[52] Nusse R and Clevers H. Wnt/β-catenin signaling, disease, and emerging therapeutic modalities. Cell 2017; 169: 985-999.

[53] Chen JF, Luo X, Xiang LS, Li HT, Zha L, Li N, He JM, Xie GF, Xie X and Liang HJ. EZH2 promotes colorectal cancer stem-like cell expansion by activating p21cip1-Wnt/β-catenin signaling. Oncotarget 2016; 7: 41540-41558.

[54] Ahn EH, Yang H, Hsieh CY, Sun W, Chang CC and Schroeder JJ. Evaluation of chemotherapeutic and cancer-protective properties of sphingosine and C2-ceramide in a human breast stem cell derived carcinogenesis model. Int J Oncol 2019; 54: 655-664.

[55] Kim SE, Cole PD, Cho RC, Ly A, Ishiguro L, Sohn KJ, Croxford R, Kamen BA and Kim YI. γ-Glutamyl hydrolase modulation and folate influence chemosensitivity of cancer cells to 5-fluorouracil and methotrexate. Br J Cancer 2013; 109: 2175-2188.

[56] Bhattacharya S, Ray RM and Johnson LR. Decreased apoptosis in polyamine depleted IEC-6 cells depends on Akt-mediated NF-κB activation but not GSK3β activity. Apoptosis 2005; 10: 759-776.

[57] Chang KY, Tsai SY, Chen SH, Tsou HH, Yen CJ, Liu KJ, Fang HL, Wu HC, Chuang BF, Chou SW, Tang CK, Liu SY, Lu PJ, Yen CY and Chang JY. Dissecting the EGFR-PI3K-AKT pathway in oral cancer highlights the role of the EGFR variant III and its clinical relevance. J Biomed Sci 2013; 20: 43.

[58] Cully M, You H, Levine AJ and Mak TW. Beyond PTEN mutations: the PI3K pathway as an integrator of multiple inputs during tumorigenesis. Nat Rev Cancer 2006; 6: 184-192.

[59] Sophia J, Kiran Kishore T K, Kowshik J, Mishra R and Nagini S. Nimbolide, a neem limonoid inhibits Phosphatidyl Inositol-3 Kinase to activate Glycogen Synthase Kinase-3β in a hamster model of oral oncogenesis. Sci Rep 2016; 6: 22192.

[60] Zhou F, Zhang L, van Laar T, van Dam H and Ten Dijke P. GSK3β inactivation induces apoptosis of leukemia cells by repressing the function of c-Myb. Mol Biol Cell 2011; 22: 3533-3540.

[61] MacDonald BT, Tamai K and He X. Wnt/β-catenin signaling: components, mechanisms, and diseases. Dev Cell 2009; 17: 9-26.

[62] Nevzorova YA, Cubero FJ, Hu W, Hao F, Haas U, Ramadori P, Gassler N, Hoss M, Strnad P, Zimmermann HW, Tacke F, Trautwein C and Liedtke C. Enhanced expression of c-myc in hepatocytes promotes initiation and progression of alcoholic liver disease. J Hepatol 2016; 64: 628-640.

[63] Stacey DW. Cyclin D1 serves as a cell cycle regulatory switch in actively proliferating cells. Curr Opin Cell Biol 2003; 15: 158-163.

TDEF inhibits H357cisR cell through PI3K/AKT/beta-catenin pathway

Supplementary Table 2. Spreadsheet data of TDEF protein profiler array for the calculation of Protein expression fold changed as compare to the expression of PBS

Targets	Array quantification values (Treatment)	Negative control (PBS)	Treatment normalized to PBS	Average	Array quantification values (Control)	Negative control (PBS)	Control normalized to PBS	Average	Fold change (Treatment avg/Control avg)
Reference spot 1	204.795	99.727	105.068		209.246	97.39	111.856		
	211.812	99.086	112.726	108.897	209.067	96.644	112.423	112.1395	0.971085122
Reference spot 2	213.697	99.727	113.97		214.448	97.39	117.058		
	216.271	99.086	117.185	115.5775	212.725	96.644	116.081	116.5695	0.991490055
Bad	119.68	99.727	19.953		118.228	97.39	20.838		
	120.598	99.086	21.512	20.7325	118.7	96.644	22.056	21.447	0.966685317
Bax	115.23	99.727	15.503		110.914	97.39	13.524		
	112.747	99.086	13.661	14.582	109.109	96.644	12.465	12.9945	1.122167071
Bcl2	103.111	99.727	3.384		102.743	97.39	5.353		
	103.62	99.086	4.534	3.959	101.675	96.644	5.031	5.192	0.76251926
Bcl-x	105.177	99.727	5.45		101.897	97.39	4.507		
	106.823	99.086	7.737	6.5935	102.977	96.644	6.333	5.42	1.216512915
Procaspase3	212.264	99.727	112.537		210.148	97.39	112.758		
	213.882	99.086	114.796	113.6665	213.551	96.644	116.907	114.8325	0.98984608
Cleaved caspase3	180.872	99.727	81.145		154.895	97.39	57.505		
	165.162	99.086	66.076	73.6105	137.413	96.644	40.769	49.137	1.49806663
catalase	147.472	99.727	47.745		129.535	97.39	32.145		
	144.953	99.086	45.867	46.806	131.205	96.644	34.561	33.353	1.403352022
cIAP1	162.231	99.727	62.504		136.504	97.39	39.114		
	160.498	99.086	61.412	61.958	139.023	96.644	42.379	40.7465	1.520572319
cIAP2	140.341	99.727	40.614		112.772	97.39	15.382		
	132.25	99.086	33.164	36.889	113.947	96.644	17.303	16.3425	2.257243384
claspin	144.25	99.727	44.523		155.091	97.39	57.701		
	140.87	99.086	41.784	43.1535	152.497	96.644	55.853	56.777	0.760052486
clusterin	105.105	99.727	5.378		100.402	97.39	3.012		
	108.322	99.086	9.236	7.307	101.79	96.644	5.146	4.079	1.791370434
cytochrome C	112.942	99.727	13.215		103.554	97.39	6.164		
	114.048	99.086	14.962	14.0885	102.869	96.644	6.225	6.1945	2.274356284
TRAIL R1/DR4	151.002	99.727	51.275		145.686	97.39	48.296		
	149.535	99.086	50.449	50.862	143.941	96.644	47.297	47.7965	1.064136495
TRAIL R2/DR5	158.281	99.727	58.554		148.467	97.39	51.077		
	157.079	99.086	57.993	58.2735	147.233	96.644	50.589	50.833	1.146371452
FADD	142.459	99.727	42.732		138.785	97.39	41.395		
	143.644	99.086	44.558	43.645	135.302	96.644	38.658	40.0265	1.090402608
Fas/TNFRSF6/CD95	178.489	99.727	78.762		154.275	97.39	56.885		
	176.267	99.086	77.181	77.9715	156.87	96.644	60.226	58.5555	1.331582857
HIF-1a	166.6	99.727	66.873		152.097	97.39	54.707		
	161.592	99.086	62.506	64.6895	149.435	96.644	52.791	53.749	1.203547973

TDEF inhibits H357cisR cell through PI3K/AKT/beta-catenin pathway

HO-1/HMOX1/HSP32	128.117	99.727	28.39		123.566	97.39	26.176		
	123.806	99.086	24.72	26.555	120.379	96.644	23.735	24.9555	1.064094087
HO-2/HMOX2	141.869	99.727	42.142		137.216	97.39	39.826		
	142.062	99.086	42.976	42.559	140.829	96.644	44.185	42.0055	1.013176846
HSP27	163.228	99.727	63.501		157.915	97.39	60.525		
	157.671	99.086	58.585	61.043	160.536	96.644	63.892	62.2085	0.981264618
HSP60	118.945	99.727	19.218		131.986	97.39	34.596		
	115.111	99.086	16.025	17.6215	125.494	96.644	28.85	31.723	0.555480251
HSP70	123.008	99.727	23.281		116.655	97.39	19.265		
	120.445	99.086	21.359	22.32	112.53	96.644	15.886	17.5755	1.269949646
HTRA/0mi	153.326	99.727	53.599		136.365	97.39	38.975		
	156.789	99.086	57.703	55.651	140.483	96.644	43.839	41.407	1.343999807
Livin	106.548	99.727	6.821		100.615	97.39	3.225		
	105.958	99.086	6.872	6.8465	99.184	96.644	2.54	2.8825	2.375195143
PON2	168.96	99.727	69.233		149.215	97.39	51.825		
	161.356	99.086	62.27	65.7515	148.347	96.644	51.703	51.764	1.270216753
p21/CIP/CDKN1 A	133.932	99.727	34.205		103.499	97.39	6.109		
	130.727	99.086	31.641	32.923	104.046	96.644	7.402	6.7555	4.873510473
p27/Kip1	110.108	99.727	10.381		104.939	97.39	7.549		
	109.168	99.086	10.082	10.2315	105.471	96.644	8.827	8.188	1.249572545
phospho-p53 (S15)	119.892	99.727	20.165		107.247	97.39	9.857		
	119.711	99.086	20.625	20.395	107.169	96.644	10.525	10.191	2.001275635
Phospho-p53 (S46)	160.032	99.727	60.305		135.575	97.39	38.185		
	156.857	99.086	57.771	59.038	134.282	96.644	37.638	37.9115	1.557258352
Phospho-p53 (S392)	144.496	99.727	44.769		127.845	97.39	30.455		
	142.374	99.086	43.288	44.0285	125.736	96.644	29.092	29.7735	1.478781467
Phospho-Rad 17 (S635)	116.181	99.727	16.454		108.025	97.39	10.635		
	116.696	99.086	17.61	17.032	108.228	96.644	11.584	11.1095	1.5331023
SMAC/Diablo	140.067	99.727	40.34		128.155	97.39	30.765		
	140.159	99.086	41.073	40.7065	128.314	96.644	31.67	31.2175	1.303964123
Survivin	132.394	99.727	32.667		148.477	97.39	51.087		
	131.259	99.086	32.173	32.42	148.962	96.644	52.318	51.7025	0.627048982
TNF RI/TNFRSF1A	112.182	99.727	12.455		109.902	97.39	12.512		
	110.143	99.086	11.057	11.756	108.523	96.644	11.879	12.1955	0.963962117
XIAP	167.962	99.727	68.235		152.703	97.39	55.313		
	171.599	99.086	72.513	70.374	158.027	96.644	61.383	58.348	1.206108179
PBS (negative control)	99.727	99.727	0		97.39	97.39	0		
	99.086	99.086	0	0	96.644	96.644	0	0	0
Reference spot	207.064	99.727	107.337		206.081	97.39	108.691		
	209.752	99.086	110.666	109.0015	206.681	96.644	110.037	109.364	0.996685381